Research Article

Humaira Yasmin*, Sana Shahab, Showkat Ahmad Lone, Zehba Raizah, and Anwar Saeed*

Convective flow of a magnetohydrodynamic second-grade fluid past a stretching surface with Cattaneo–Christov heat and mass flux model

https://doi.org/10.1515/phys-2023-0204
received November 14, 2023; accepted February 09, 2024

Abstract: This research delves into dynamics of magnetohydrodynamic second-grade fluid flow influenced by the presence of gyrotactic microorganisms on a stretching sheet. The study takes into account various factors such as thermal radiation, chemical reactivity, and activation energy, all of which contribute to the complex behavior of fluid flow in this system. The interaction between the magnetic field and the fluid, combined with the biological aspect introduced by gyrotactic microorganisms, adds complexity to the overall analysis. The mathematical model is presented in the form of partial differential equations (PDE)s. Using the similarity variables, the modeled PDEs are transformed into ordinary differential equations. Homotopy analysis method is used for the solution of the modeled equations. After a detailed insight into this investigation, it is established that the velocity distribution declined for growth in magnetic factor and second-grade fluid parameter. The thermal characteristics are augmented for the greater values of radiation, thermophoretic and Brownian motion factors, while these profiles are weakened for upsurge in thermal relaxation time factor and Prandtl number. The concentration characteristics declined with the enhancement in Schmidt number, mass relaxation time, chemical reaction, and Brownian motion factors, while they amplified with enhancement in activation energy and thermophoresis factors. The microorganisms' profiles are the declining functions of bioconvection Lewis and Peclet numbers. This study included a comparative analysis, which aligns closely with existing research, demonstrating a strong concordance with established findings.

Keywords: non-Newtonian fluid, Fourier's and Fick's laws, activation energy, gyrotactic microorganisms, thermal radiation, chemical reaction, (HAM)

*** Corresponding author: Humaira Yasmin**, Department of Basic Sciences, General Administration of Preparatory Year, King Faisal University, Al Ahsa 31982, Saudi Arabia, e-mail: hhassain@kfu.edu.sa
*** Corresponding author: Anwar Saeed**, Department of Mathematics, Abdul Wali Khan University, Mardan, 23200, Khyber Pakhtunkhwa, Pakistan, e-mail: anwarsaeed769@gmail.com
Sana Shahab: Department of Business Administration, College of Business Administration, Princess Nourah Bint Abdulrahman University, P.O. Box 84428, Riyadh 11671, Saudi Arabia
Showkat Ahmad Lone: Department of Basic Sciences, College of Science and Theoretical Studies, Saudi Electronic University, (Jeddah-M), Riyadh-11673, Saudi Arabia
Zehba Raizah: Department of mathematics, College of Science, King Khalid University, Abha, Saudi Arabia

Nomenclature

u, v	velocity components
x, y	coordinates
B_0	strength of magnetic field
u_w	stretching velocity
T, T_f, T_∞	surface, fluid, and free stream temperature
C, C_f, C_∞	surface, fluid, and free stream concentration
H, H_f, H_∞	surface, fluid, and free stream microorganism concentration
h_f	heat transfer coefficient
h_g	mass transfer coefficient of the nanoparticles
h_m	mass transfer coefficient of the microorganisms
λ	second-grade fluid parameter
M	magnetic factor
γ_1	thermal Biot number
γ_2	nanoparticle concentration Biot number
γ_3	microorganism concentration Biot number
Nb	Brownian motion factor
Nt	thermophoresis factor
Pr	Prandtl number
Rd	radiation factor
Sc	Schmidt number

E	activation energy
Pe	Peclet number
Le	Lewis number
δ	concentration difference factor
a	stretching constant
α_e, α_c	thermal and mass relaxation time factors
D_B, D_T, D_m	Brownian, thermophoresis, and microorganism diffusion coefficients
Nu_x, Sh_x, Nm_x	Nusselt, Sherwood, and microorganism density numbers
σ_T	temperature difference factor

Abbreviations

PDEs, ODEs	partial and ordinary differential equations
SWCNTs	single-wall carbon nanotubes
MHD	magneto-hydrodynamics
EMHD	electro-magneto-hydrodynamics
HAM	homotopy analysis method

1 Introduction

During past few decades, non-Newtonian fluid has turn into a significant field of inquiry as such fluid has widespread applications in technology and engineering, for instance, biological liquid motion, lubricants' production, and plastics fabrication. Such fluids are highly viscous and are extensively used in various fabrication phenomena. Biswal *et al.* [1] considered radiated non-Newtonian fluid motion on a nonlinear elongating sheet and concluded that with expansion in magnetic effects, the velocity panels have deteriorated. Iqbal *et al.* [2] analyzed thermal transportation for Maxwell fluid flow on a vertically elongating sheet with impacts of heat and mass flux model suggested by Cattaneo–Christov. Sharma and Shaw [3] have explored non-Newtonian magneto-hydrodynamics (MHD) liquid motion over an elongating sheet that is affected by nonlinearly radiated as well as viscously dissipated influence and have deduced that the fluid motion, temperature as well as mass diffusions have not been remained consistent in case of non-Newtonian liquid motion. Iqbal and Saleem [4] explained convective thermal transportation phenomenon of Casson flow of fluid through a vertical conduit and noted that thermal panels have augmented for expansion in Eckert number. Khalil *et al.* [5] have discussed the impacts of non-Newtonian fluid flow upon a stretched sheet using the effects of varying fluid characteristics upon the fluid motion and have emphasized that improvement in Deborah number has degenerated the concentration characteristics. Nandi *et al.* [6] have discussed computationally MHD Carreau nanofluid flow on a stretching sheet with optimization of entropy and have noted that velocity distribution has deteriorated with escalation in Weissenberg number. Asogwa *et al.* [7] debated on non-Newtonian electro-magneto-hydrodynamics (EMHD) fluid flow on a Riga surface using ramped energy and have proved that with growth in Schmidt and Prandtl numbers, the Sherwood and Nusselt numbers have been augmented. Farahani *et al.* [8] inspected the governing non-Newtonian flow of fluid with thermal transportation through a channel by employing triangular porous ribs. Rehman *et al.* [9] scrutinized mathematically the non-Newtonian fluid flow on an elongating sheet with dual stratified effects and have proved that velocity distribution has improved with upsurge in material factor.

The Fourier's law of thermal conduction is a substantial model that is applied in physics for mass as well as thermal transportation processes. There are numerous industrial and engineering applications of these processes, such as coolant of electric devices and processing of food. Fourier [10] has deliberated on heat transportation phenomenon, whereas Fick [11] has exposed the transportation of mass. But these phenomena [11] were not appropriate due to the fact that deviations in relaxation have been affected critically by diffusions of mass as well as temperature. As a consequence, Cattaneo [12] has modified these concepts that were improved further by Christov [13]. Waqas *et al.* [14] have debated on numerical solution for nano-liquid using the influence of heat flux and concluded that temperature flow has diminished with expansion in Cattaneo and Christov factors. Gireesha *et al.* [15] examined the consequences of Cattaneo–Christov model of heat/mass flux and noted that fluid heat flow properties have decayed with the augmentation of Cattaneo–Christov components. Reddy *et al.* [16] deliberated the Cattaneo–Christov model of heat/mass flux characteristics for nanofluid flow upon gyrating cylinder and concluded that temperature has been weakened with intensification in temperature slip factor. The influences of Cattaneo–Christov model of heat flux upon MHD Maxwell nanoparticle flow upon bi-directional stretching sheet were scrutinized in a previous study [17]. Related ideas can be perceived in previous studies [18–23].

The least quantity of energy that is needed for origination of a reaction is identified as activation energy. In the process of mass transportation, the mutual effects of chemical reactivity and activation energy are quite significant. This concept has widespread applications at industrial level, such as coolant of nuclear reactant, thermal oil recovery, chemical engineering, and geothermal reservoirs. Raza-E-Rabbi *et al.* [24] scrutinized MHD fluid flow

using activated energy as well as nonlinear radiations and have concluded that with growth in thermophoresis and Brownian factors, the temperature is upsurge. Zeeshan *et al.* [25] studied numerically the consequences of MHD on flow of nano-liquid on penetrable stretched cylinder with impact of activated energy and deduced that with upsurge in activation energy parameter, the Sherwood number has grown up. Khan *et al.* [26] have inspected bio-convective nanofluid flow with activated energy and viscously dissipated effects and underlined that mass diffusion has dropped with thermophoretic and Brownian factors, whereas it has supported by growth in activation energy factor. Azam [27] has inspected nonlinearly thermally radiated Maxwell MHD fluid flow using activation energy as well as the influence of Cattaneo–Christov model of heat flux. Kumar *et al.* [28] have debated on the fabrication of entropy for slip fluid flow of nanoparticles past a gyrating disk for nonlinearly mixed convective activation energy.

The collection of microorganism is combined with a fluid for the prevention of particles accumulation. For improved bio-convection phenomenon, a better fluid mixture is needed, that is why, microorganisms are added to fluid. The phenomenon of bio-convection is a consequence of density gradient of microorganism. This process has extensive applications, for instance, oil recovery technique, oil and gas industry, and cancer treatment. Bhatti *et al.* [29] deliberated on spinning of microorganism in nanofluid flow through gyratory plates, placed in a permeable medium, and have concluded that growth in Peclet number has augmented the profiles of microorganism, whereas it has supported by the upsurge in bio-convective Schmidt number. Upreti *et al.* [30] have explored the Buongiorno model effects on flow of MHD nanoparticles on a Riga surface with influence of microorganisms and exposed that thermal flow amplified, whereas fluid velocity has declined for expansion in magnetic factor. The thermal behavior of nanofluid in a permeable conduit using the influence of microbes' presence upon liquid motion was considered in a previous study [31]. Khan *et al.* [32] scrutinized bio-convective nano-liquid flow past a thin rotary needle. Faizan *et al.* [33] have surveyed the formation of entropy and flow of fluid on a Riga surface using gyrotactic microorganisms and proved that velocity panels upsurge with Deborah number. Madhukesh *et al.* [34] debated on nanoparticle flow with the influence of carbon nanotubes (CNTs) and microorganisms on a Riga surface using heat sink/source.

Thermal radiations are produced whenever heat is converted to EMHD radiations during the movement of charge particles in the materials. Rehman *et al.* [35] discussed a relative work on thermal transportation for MHD fluid flow subjected to thermal radiations upon plane as well as cylindrical surfaces and have concluded that the thermal distribution is higher for cylindrical surface. Hussain *et al.* [36] have discussed that the temperature distribution has improved with upsurge in radiation. Shaw *et al.* [37] have explored hydro-magnetic flow of fluid using thermal radiations and arbitrary Prandtl number and emphasized that thermal distributions have amplified with progression in radiations factor for Prandtl number in the range $10^{-10} \leq \mathrm{Pr} \leq 10^{4}$. Lone *et al.* [38] argued on MHD fluid flow on a surface with thermal radiation effects and presumed that thermal panels have been improved with upsurge in Eckert number as well as magnetic and radiation factors. Ibrahim *et al.* [39] surveyed on MHD liquid flow along a stretching plate subject to thermal radiations. Bilal *et al.* [40] observed the influences of thermal radiations on a stretched permeable sheet. Dogonchi *et al.* [41] scrutinized the water-based nanoparticle flow amid two triangular enclosures. Further related studies can be perceived in previously published works [17,42–45]. Adnan *et al.* [46] inspected the thermal performance stagnant point nanofluid flow on a permeable and vertically placed cylinder with impacts of nonlinear thermal radiations. Turkyilmazolu [47] inspected the fluid flow on porous slider and has discovered that when a flat slider expands, it reduces lift and drag, while the opposite occurs when it contracts. This has practical implications as expanding the slider can result in less frictional resistance during operation. Rehman *et al.* [48] surveyed on MHD 3D flow of nanofluid on a rotary disk by considering uniform suction with outcome as dominant behavior of magnetic factor on velocity distribution. Turkyilmazolu [49] focused on thermal transference development capability for the Cattaneo–Christov heat flux model, with the incorporation of non-Fourier effects. Muhammad *et al.* [50] discussed computationally partial differential equation (PDE) hydrodynamics fluid flow using finite volume method.

The homotopy analysis method (HAM) stands as a powerful and flexible analytical approach for addressing nonlinear differential equations [51,52]. At its core, HAM capitalizes on the concept of constructing a homotopy a continuous mapping from a known, solvable problem to the target nonlinear problem. The essence of HAM lies in its ability to transform a complex nonlinear problem into a more manageable one by introducing an auxiliary linear problem [53]. HAM's versatility is exemplified by its successful application across diverse fields such as fluid dynamics, heat transfer, biology, and engineering, where nonlinearities abound. Notably, the method's analytical nature allows researchers to derive explicit expressions, providing not only solutions but also valuable insights into the underlying physical phenomena. Its efficiency, combined with the adaptability to various nonlinear scenarios, positions HAM as a valuable tool in the

researcher's arsenal [54]. Furthermore, HAM's educational value cannot be overstated, serving as a pedagogical instrument to elucidate the intricacies of analytical methods for nonlinear problem-solving. HAM represents a sophisticated yet accessible analytical framework that has proven instrumental in unraveling the complexities of nonlinear systems across scientific and engineering disciplines. This approach provides the solution in function series form [55].

This study explores for the first time the convective flow of a second-grade fluid on a stretching surface, incorporating the Cattaneo–Christov model for heat and mass flux with impacts of gyrotactic microorganisms, thermal radiations along with chemically reactivity, thermophoresis, Brownian motion, and activated energy. The magnetic field impact is also considered in this work. In this investigation, a mathematical model is meticulously formulated in PDE form and then converted to ordinary differential equations (ODEs) using appropriate variables. Finally, HAM becomes instrumental in solving these transformed equations. This work will answer the following research questions:

1) How does the inclusion of the Cattaneo–Christov heat and mass flux model influence the convective flow characteristics of a second-grade fluid?
2) What role does the stretching surface play in shaping the convection patterns of the second-grade fluid, considering the Cattaneo–Christov model for heat and mass flux?
3) How do the Cattaneo–Christov parameters impact the heat and mass transfer processes in the convective flow on the elongating sheet?
4) What are the impacts of emerged factors on the flow panels when the nanofluid flows over a stretching surface?
5) What are the impacts of the emerged factors on the heat and mass transfer rates and density number?

Thus, to engage with the above research questions, a mathematical model for the proposed flow problem is designed, which is specified in Section 2. The solution of the modeled equations is described in Section 3. The discussion is presented in Section 4. Finally, the outcomes of current analysis are shown in Section 5.

2 Formulation of the problem

Consider the flow of an incompressible second-grade fluid on an elongating sheet. The velocity of stretching surface, denoted by $u_w = ax$, is taken along x-direction, while y-axis is normal to the fluid flow. u and v are the velocity components along x- and y-directions, respectively. T, T_w, and T_∞ represent the temperature, surface temperature, and free-stream temperature, respectively. Similarly C, C_w, and C_∞ represent the nanoparticle concentration, surface concentration, and free-stream concentration, respectively. Also, H, H_w, and H_∞ represent the microorganism concentration, microorganism surface concentration, and microorganism free-stream concentration, respectively. A magnetic field of strength B_0 is applied normal to the fluid flow (along y-axis). The Cattaneo–Christov heat and mass flux model is considered to investigate the heat and mass transfer rates. Furthermore, the thermophoresis, Brownian motion, chemical reaction, and activation energy impacts are taken into consideration. Convective conditions at the surface of the sheet are considered in this analysis. By employing the aforementioned assumptions, we have the following equations [55–58] (Figure 1):

$$\frac{\partial u}{\partial x} + \frac{\partial v}{\partial y} = 0, \tag{1}$$

$$u\frac{\partial u}{\partial x} + v\frac{\partial u}{\partial y} = \frac{\mu}{\rho}\frac{\partial^2 u}{\partial y^2} + \frac{\alpha_1}{\rho}\left[u\frac{\partial^3 u}{\partial x \partial y^2} + \frac{\partial u}{\partial x}\frac{\partial^2 u}{\partial y^2} + v\frac{\partial^3 u}{\partial y^3} - \frac{\partial u}{\partial y}\frac{\partial^2 v}{\partial y^2}\right] - \frac{\sigma B_0^2}{\rho}u, \tag{2}$$

$$u\frac{\partial T}{\partial x} + v\frac{\partial T}{\partial y} = \frac{1}{(\rho C_p)}\left(k + \frac{16\sigma^* T_\infty^3}{3k^*}\right)\frac{\partial^2 T}{\partial y^2} + \tau\left(D_B\frac{\partial C}{\partial y}\frac{\partial T}{\partial y} + \frac{D_T}{T_\infty}\frac{\partial T}{\partial y}\frac{\partial C}{\partial y}\right) - \alpha_2\left(u\frac{\partial T}{\partial x}\frac{\partial u}{\partial x} + v\frac{\partial v}{\partial y}\frac{\partial T}{\partial y} + v^2\frac{\partial^2 T}{\partial y^2} + u^2\frac{\partial^2 T}{\partial x^2} + 2vu\frac{\partial^2 T}{\partial x \partial y} + u\frac{\partial T}{\partial y}\frac{\partial v}{\partial x} + v\frac{\partial T}{\partial x}\frac{\partial u}{\partial y}\right), \tag{3}$$

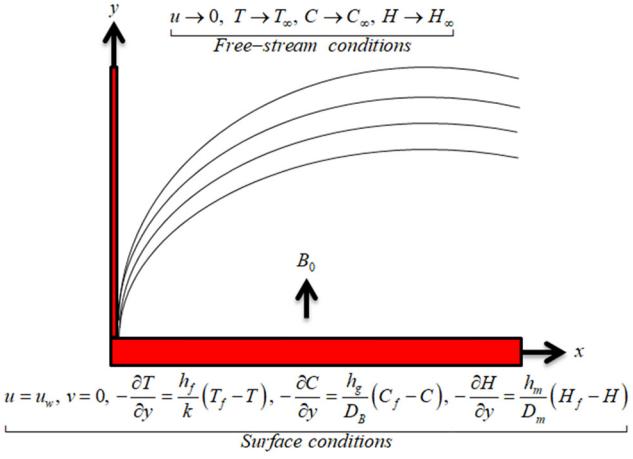

Figure 1: Geometrical view of flow.

$$
\begin{aligned}
&u\frac{\partial C}{\partial x} + v\frac{\partial C}{\partial y} \\
&= D_{\mathrm{B}}\frac{\partial^2 C}{\partial y^2} + \frac{\partial^2 T}{\partial y^2}\frac{D_T}{T_\infty} - k_{\mathrm{r}}^2(C - C_\infty)\left(\frac{T}{T_\infty}\right)^n \exp\left[-\frac{E_{\mathrm{a}}}{k_{\mathrm{B}}T}\right] \\
&\quad - \alpha_3\left(u\frac{\partial C}{\partial x}\frac{\partial u}{\partial x} + v\frac{\partial v}{\partial y}\frac{\partial C}{\partial y} + v^2\frac{\partial^2 C}{\partial y^2} + u^2\frac{\partial^2 C}{\partial x^2}\right. \\
&\quad \left. + 2uv\frac{\partial^2 C}{\partial x \partial y} + u\frac{\partial C}{\partial y}\frac{\partial v}{\partial x} + v\frac{\partial C}{\partial x}\frac{\partial u}{\partial y}\right),
\end{aligned} \tag{4}
$$

$$
\begin{aligned}
&u\frac{\partial H}{\partial x} + v\frac{\partial H}{\partial y} + \frac{b_{\mathrm{c}}W_{\mathrm{c}}}{(C_{\mathrm{f}} - C_\infty)}\frac{\partial C}{\partial y}\frac{\partial H}{\partial y} + \frac{b_{\mathrm{c}}W_{\mathrm{c}}}{(C_{\mathrm{f}} - C_\infty)}H\frac{\partial^2 C}{\partial y^2} \\
&\quad = D_{\mathrm{m}}\frac{\partial^2 H}{\partial y^2}.
\end{aligned} \tag{5}
$$

Boundary conditions are described as [59]:

$$
\begin{cases}
v = 0, u = u_{\mathrm{w}}, -\dfrac{\partial T}{\partial y} = \dfrac{h_{\mathrm{f}}}{k}(T_{\mathrm{f}} - T), \\
-\dfrac{\partial C}{\partial y} = \dfrac{h_{\mathrm{g}}}{D_{\mathrm{B}}}(C_{\mathrm{f}} - C), -\dfrac{\partial H}{\partial y} = \dfrac{h_{\mathrm{m}}}{D_{\mathrm{m}}}(H_{\mathrm{f}} - H) \ \text{ at } y = 0, \\
u \to 0, H \to H_\infty, C \to C_\infty, T \to T_\infty, \ \text{ as } y \to \infty.
\end{cases} \tag{6}
$$

In the aforementioned equations, μ is the dynamic viscosity, ρ is the density, α_1 is the material parameter, σ is the electrical conductivity, C_{p} is the specific heat, k is the thermal conductivity, σ^* is the Stefan–Boltzmann constant, k^* is the mean absorption coefficient, D_{B} is the coefficient of nanoparticles' Brownian diffusion, D_{T} is the thermophoretic coefficient, α_2 is the relaxation time of heat diffusion, α_3 is the relaxation time of mass diffusion, k_{r} is the chemical reaction coefficient, E_{a} is the activation energy coefficient, b_{c} is the chemotaxis coefficient, W_{c} is the maximum cell swimming speed, D_{m} is the Brownian diffusion of microorganisms, h_{f} is the heat transfer coefficient, h_{g} is the nanoparticle's mass transfer coefficient, and h_{m} is the microorganisms' mass transfer coefficient.

The transformable variables are depicted as:

$$
\begin{aligned}
&u = bxf'(\eta), v = -\sqrt{\upsilon_{\mathrm{f}}b}f(\eta), \psi(\eta) = \frac{H - H_\infty}{H_{\mathrm{f}} - H_\infty}, \\
&\theta(\eta) = \frac{T - T_\infty}{T_{\mathrm{f}} - T_\infty}, \Phi(\eta) = \frac{C - C_\infty}{C_{\mathrm{f}} - C_\infty}, \eta = \sqrt{\frac{b}{\upsilon_{\mathrm{f}}}}y.
\end{aligned} \tag{7}
$$

Using the aforementioned similarity transformations, we have the following:

$$
\begin{aligned}
&f'''(\eta) + f''(\eta)f(\eta) - f'^2(\eta) + \lambda(f'''(\eta)f'(\eta) - f(\eta)f^{\mathrm{iv}}(\eta) \\
&\quad - (f''(\eta))^2) - Mf'(\eta) = 0,
\end{aligned} \tag{8}
$$

$$
\begin{aligned}
&\frac{1}{\mathrm{Pr}}(1 + \mathrm{Rd})\theta''(\eta) + \theta'(\eta)f(\eta) + \mathrm{Nb}\Phi'(\eta)\theta'(\eta) \\
&\quad + \mathrm{Nt}\theta'^2(\eta) - \alpha_{\mathrm{e}}(f'^2(\eta)\theta(\eta) - f(\eta)f''(\eta)\theta(\eta) \\
&\quad - \theta'(\eta)f'(\eta)f(\eta) + \theta''(\eta)f^2(\eta)) = 0,
\end{aligned} \tag{9}
$$

$$
\begin{aligned}
&\Phi''(\eta) - \mathrm{Sc}\alpha_{\mathrm{c}}(f'^2(\eta)\Phi(\eta) - f(\eta)(f''(\eta)\Phi(\eta) - f'(\eta)\Phi'(\eta)) \\
&\quad + f^2(\eta)\Phi''(\eta)) + \frac{\mathrm{Nt}}{\mathrm{Nb}}\theta''(\eta) + \mathrm{Sc}f(\eta)\Phi'(\eta) \\
&\quad - \mathrm{Sc}\varpi\Phi(\eta)(\sigma\theta(\eta) + 1)^n \exp\left(-\frac{E}{\sigma\theta(\eta) + 1}\right) = 0,
\end{aligned} \tag{10}
$$

$$
\begin{aligned}
&\psi''(\eta) + \mathrm{Lb}\psi'(\eta)f(\eta) - \mathrm{Pe}(\psi'(\eta)\Phi'(\eta) + \Phi''(\eta)\psi(\eta) \\
&\quad + \delta\Phi''(\eta)\varphi''(\eta)) = 0,
\end{aligned} \tag{11}
$$

with related constraints at boundaries

$$
\begin{cases}
f'(\eta = 0) = 1, f(\eta = 0) = 0, f'(\eta \to \infty) \to 0, \\
\theta'(\eta = 0) = -\gamma_1(1 - \theta(\eta = 0)), \theta(\eta \to \infty) \to 0, \\
\Phi'(\eta = 0) = -\gamma_2(1 - \Phi(\eta = 0)), \Phi(\eta \to \infty) \to 0, \\
\psi'(\eta = 0) = -\gamma_3(1 - \psi(\eta = 0)), \psi(\eta \to \infty) \to 0.
\end{cases} \tag{12}
$$

In the aforementioned equations, $\lambda\left(=\frac{\alpha_1 b}{\mu}\right)$ is the second-grade fluid parameter; $M\left(=\frac{\sigma B_0^2}{\rho b}\right)$ is the magnetic factor; $\gamma_1\left(=\frac{h_{\mathrm{f}}}{k}\sqrt{\frac{\upsilon}{b}}\right)$, $\gamma_2\left(=\frac{h_{\mathrm{g}}}{D_{\mathrm{B}}}\sqrt{\frac{\upsilon}{b}}\right)$, and $\gamma_3\left(=\frac{h_{\mathrm{m}}}{D_{\mathrm{m}}}\sqrt{\frac{\upsilon}{b}}\right)$ are the thermal, concentration, and microorganism concentration of Biot numbers, respectively; $\alpha_{\mathrm{e}}(=b\alpha_2)$ and $\alpha_{\mathrm{c}}(=b\alpha_3)$ are the thermal and mass relaxation time factors, respectively; $\mathrm{Nt}\left(=\frac{\tau D_{\mathrm{T}}(T_{\mathrm{f}} - T_\infty)}{\upsilon T_\infty}\right)$ is the thermophoresis factor; $\mathrm{Nb}\left(=\frac{\tau D_{\mathrm{B}}(C_{\mathrm{f}} - C_\infty)}{T_\infty}\right)$ is the Brownian motion factor; $\mathrm{Rd}\left(=\frac{16\sigma^* T_\infty^3}{3k^*}\right)$ is the thermal radiation factor; $\mathrm{Sc}\left(=\frac{\upsilon}{D_{\mathrm{B}}}\right)$ is the Schmidt number; $\sigma_{\mathrm{T}}\left(=\frac{T_{\mathrm{f}} - T_\infty}{T_\infty}\right)$ is the temperature difference factor; $\mathrm{Pr}\left(=\frac{\upsilon(\rho C_{\mathrm{p}})}{k}\right)$ is the Prandtl number; $E\left(=\frac{E_{\mathrm{a}}}{k_{\mathrm{B}}T_\infty}\right)$ is the activation energy factor; $\mathrm{Pe}\left(=\frac{b_{\mathrm{c}}W_{\mathrm{c}}}{D_{\mathrm{m}}}\right)$ is the Peclet number; $\mathrm{Lb}\left(=\frac{\upsilon}{D_{\mathrm{m}}}\right)$ is the Lewis number; and $\delta\left(=\frac{H_{\mathrm{f}} - H_\infty}{H_\infty}\right)$ is the concentration difference factor.

The interested engineering quantities are described as:

$$
\mathrm{Nu}_x = -\frac{x}{k(T_{\mathrm{f}} - T_\infty)}\left(k + \frac{16\sigma^* T_\infty^3}{3k^*}\right)\left.\frac{\partial T}{\partial y}\right|_{y=0}, \tag{13}
$$

$$\mathrm{Sh}_x = -\frac{x}{D_B(C_f - C_\infty)}\frac{\partial C}{\partial y}\bigg|_{y=0}, \tag{14}$$

$$\mathrm{Nm}_x = -\frac{x}{D_m(N_f - N_\infty)}\frac{\partial N}{\partial y}\bigg|_{y=0}. \tag{15}$$

Eqs. (14–16) are reduced as:

$$\frac{\mathrm{Nu}_x}{\sqrt{\mathrm{Re}_x}} = -(1 + \mathrm{Rd})\theta'(0). \tag{16}$$

$$\frac{\mathrm{Sh}_x}{\sqrt{\mathrm{Re}_x}} = -\Phi'(0). \tag{17}$$

$$\frac{\mathrm{Nm}_x}{\sqrt{\mathrm{Re}_x}} = -\psi'(0). \tag{18}$$

3 HAM solution

HAM is a semi-numerical approach used for solving nonlinear differential equations. Introduced by Prof. Shijun Liao in the early 1990s, HAM involves constructing a homotopy, a continuous deformation from a known, easily solvable problem to the original nonlinear problem. This is achieved by introducing an embedding parameter, and the solution is expressed as a series in powers of this parameter. The homotopy equation combines the original nonlinear problem with an auxiliary linear problem, and as the parameter varies, the solution deforms from the known solution of the linear problem to the desired solution of the nonlinear problem.

3.1 Advantages of HAM

- The method follows a systematic and iterative process, constructing a homotopy and obtaining solutions through a series expansion. This allows for a step-by-step understanding and refinement of the solution.
- HAM often provides physical insights into the problem by revealing the influence of different parameters on the solution. This interpretability is particularly valuable in understanding complex nonlinear phenomena.
- The method incorporates an auxiliary convergence control parameter, allowing researchers to adjust the convergence rate of the solution. This feature contributes to the flexibility and adaptability of HAM.
- HAM is known for its efficiency in producing accurate results, especially in situations where other analytical methods may face challenges. It is particularly well suited for problems with strong nonlinearities.
- HAM complements numerical methods by providing analytical insights into the problem. This can be crucial for gaining a deeper understanding of the underlying dynamics and mechanisms.
- HAM is capable of handling complex nonlinear problems that may be challenging for other analytical methods. Its flexibility allows researchers to tackle problems with various forms of nonlinearity.
- The analytical nature of HAM often leads to reduced computational costs compared to numerical methods. This is particularly advantageous in scenarios where computational resources are limited.

For solution of Eqs. (8–11) along with Eq. (12), the HAM approach has used. This approach needs starting values, which are described below:

$$\left.\begin{aligned} &f_0(\eta) = 1 - e^{-\eta},\ \theta_0(\eta) = \frac{\gamma_1}{1+\gamma_1}(e^{-\eta}),\\ &\Phi_0(\eta) = \frac{\gamma_2}{1+\gamma_2}(e^{-\eta}),\ \psi_0(\eta) = \frac{\gamma_3}{1+\gamma_3}(e^{-\eta}). \end{aligned}\right\} \tag{19}$$

$$\left.\begin{aligned} &L_f[f(\eta)] = f'''(\eta) - f'(\eta),\\ &L_\theta[\theta(\eta)] = \theta''(\eta) - \theta(\eta),\\ &L_\Phi[\Phi(\eta)] = \Phi''(\eta) - \Phi(\eta),\\ &L_\psi[\psi(\eta)] = \psi''(\eta) - \psi(\eta). \end{aligned}\right\} \tag{20}$$

with

$$\left.\begin{aligned} &L_f[\Im_1 + \Im_2 e^{(-\eta)} + \Im_3 e^{(\eta)}] = 0,\\ &L_\theta[\Im_4 e^{(-\eta)} + \Im_5 e^{(\eta)}] = 0,\\ &L_\Phi[\Im_6 e^{(-\eta)} + \Im_7 e^{(\eta)}] = 0,\\ &L_\psi[\Im_8 e^{(-\eta)} + \Im_9 e^{(\eta)}] = 0. \end{aligned}\right\} \tag{21}$$

where $\Im_1$–$\Im_9$ are the fixed values.

3.2 Convergence of HAM

For convergence of HAM has the auxiliary factors, which are described by $\hbar_f$, $\hbar_\theta$, $\hbar_\phi$, and $\hbar_\psi$. In this method, the region of convergence has been established by employing $\hbar$-curves corresponding to a 15th order of approximation, as illustrated in Figure 2. It has been noted from this figure that the zone of velocity convergence is $-3.1 \le \hbar_f \le 0.0$, for temperature, it is $-3.5 \le \hbar_\theta \le 0.5$, while for concentration, it is given by the range $-3.0 \le \hbar_\Phi \le 0.5$. Moreover, the zone of convergence for motile panels is given as $-2.9 \le \hbar_\psi \le 0.5$.

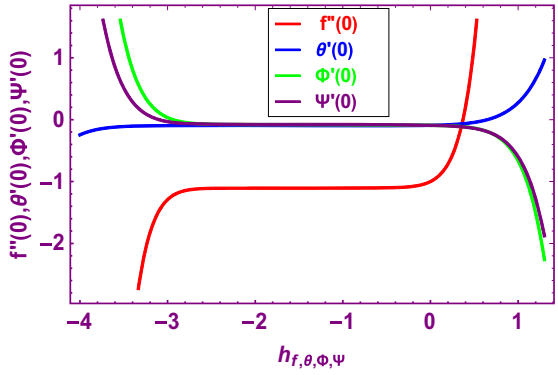

Figure 2: h-curves for $f''(0)$, $\theta'(0)$, $\Phi'(0)$, and $\psi'(0)$.

4 Results and discussions

This study investigated the second-grade fluid flow encompassing gyrotactic microbes on a stretched sheet. The fluid flow is affected by thermal radiation, chemical reactivity, and activation energy factors. The Cattaneo–Christov thermal and mass flux model is also incorporated in the considered flow problem. During the non-dimensionalization process of the modeled equations, some dimensionless factors are found, and the foremost aim of this analysis is to study the influences of these factors on the flow profiles. The default values of the embedded factors are chosen as $\lambda = 0.6$, $M = 1.3$, $\gamma_1 = 0.5$, $\gamma_2 = 0.5$, $\gamma_3 = 0.5$, $\alpha_e = 0.7$, $\alpha_c = 0.6$, Nt = 0.1, Rd = 0.3, Nb = 0.1, Pr = 0.72, Sc = 0.5, $\sigma_T = 1.1$, $E = 1.0$, Pe = 1.5, Le = 1.1, and $\delta = 1.1$. The impact of these parameters on various panels of flow will be deliberated in forthcoming paragraph.

4.1 Velocity characteristics

The effects of several emerging factors upon the velocity profiles of fluid are discussed graphically in Figures 3(a) and (b). In Figure 3(a), it is detected that with improvement in magnetic factor M, the fluid motion declines. It is because of the fact that greater M generates the Lorentz force, which retards the fluid motion. The contrasting force that is produced due to Lorentz force increases the friction force at the sheet's surface and causes a reduction in the fluid velocity. Therefore, the greater M reduces the velocity characteristic, as depicted in Figure 3(a). In Figure 3(b), the influence of second-grade fluid parameter λ on the velocity panels is displayed. In this figure, it is observed that fluid motion upsurges with the growth in λ. The second-grade fluid parameter characterizes the material's rheological properties, impacting its response to shear stress. As λ grows, the fluid exhibits a more pronounced

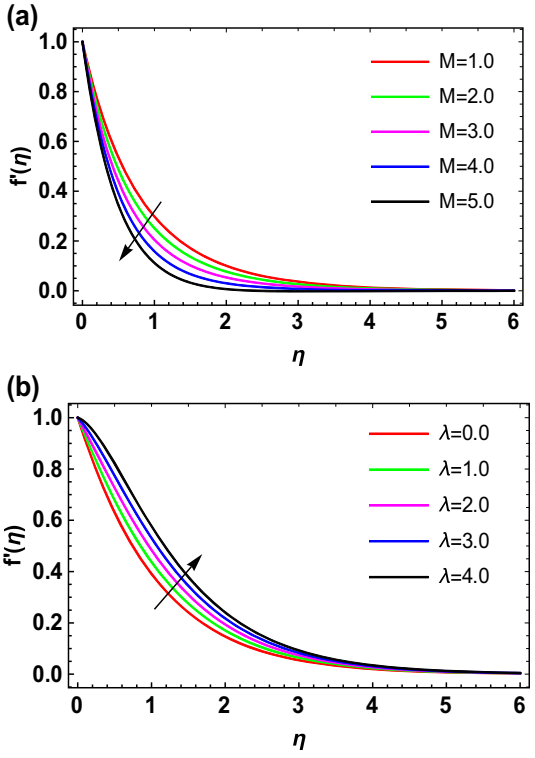

Figure 3: (a) Impact of magnetic factor M on velocity distribution $f'(\eta)$, and (b) impact of second-grade fluid factor λ on velocity distribution $f'(\eta)$.

shear-thinning behavior, leading to enhanced velocity gradients. Consequently, the overall velocity distribution across the fluid is heightened. Hence, expansion in λ causes intensification in fluid motion, as shown in Figure 3(b).

4.2 Temperature characteristics

The impression of numerous flow parameters upon temperature characteristic is shown in Figure 4(a)–(e). The effect of Rd on energy curve is shown in Figure 4(a). It is detected in Figure 4(a) that with the growth in Rd, there is an augmentation in thermal panels. Actually, as the thermal radiation factor rises, the emission of electromagnetic waves also increases, signifying a greater release of thermal energy. This heightened radiation contributes to an elevated thermal distribution across the system, resulting in increased temperatures. The interpretation underscores the direct relationship between the thermal radiation factor and the thermal profile, emphasizing the influential role of radiative heat transfer in shaping temperature distributions within the system. In Figure 4(b), the impact of Pr on temperature characteristic is described. It is apparent from this figure that thermal flow declines for

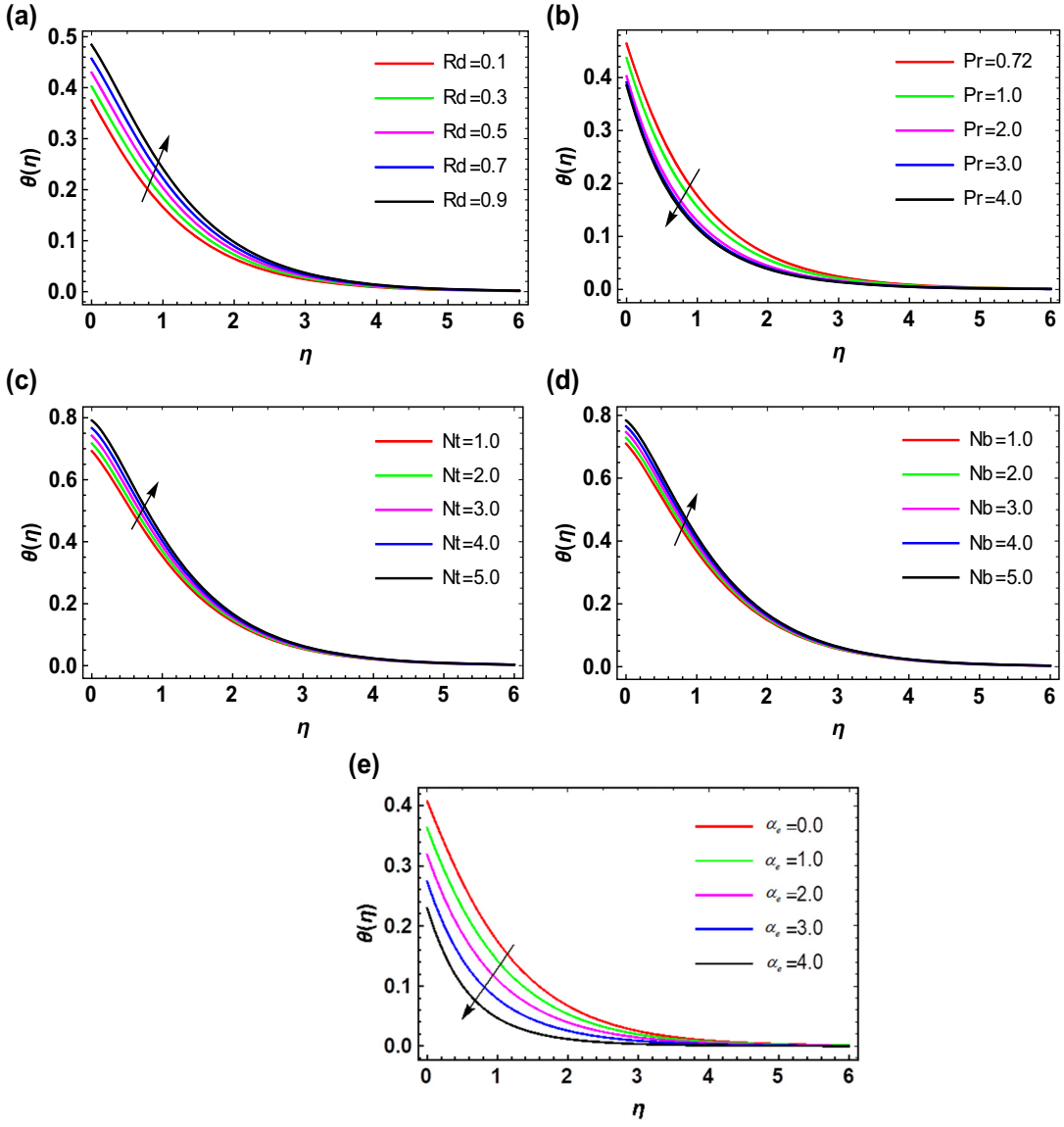

Figure 4: (a) Impact of thermal radiation factor Rd on temperature distribution $\theta(\eta)$, (b) impact of Pr on energy profile $\theta(\eta)$, (c) impact of thermophoresis factor Nt on temperature distribution $\theta(\eta)$, (d) impact of Brownian motion factor Nb on temperature distribution $\theta(\eta)$, and (e) impact of thermal relaxation time factor α_e on temperature distribution $\theta(\eta)$.

expansion in Pr. This can be explained physically as Pr that gives the ratio of momentum diffusivity to thermal diffusivity, which influences the efficiency of heat transfer in the fluid. A higher Prandtl number suggests the reduced thermal diffusivity relative to momentum diffusivity, slowing down thermal distribution. This phenomenon implies that heat transfer becomes less effective, leading to a delayed spread of thermal energy within the fluid as portrayed in Figure 4(b). The impact of thermophoresis factor Nt upon temperature characteristic is illustrated in Figure 4(c). Since in case of thermophoresis factor we have mathematically as $\mathrm{Nt} = \tau D_T(T_f - T_\infty)/\upsilon T_\infty$, which can be interpreted as for grater values of Nt, there is higher gradient in temperature between the thermal diffusion at surface of sheet to free stream. Hence, due to the growth in Nt, more heat diffuses, which supports the strength of thermal layer at boundary. Therefore, with higher values of Nt, temperature characteristic upsurges as portrayed in Figure 4(c). The impact of Nb upon fluid temperature is portrayed in Figure 4(d). It is professed in this figure that with the expansion in Nb, the temperature profile augments. Actually, for higher values of Nb, there are more collisions among the nanoparticles due to which more heat diffuses. Because during the growth in

Brownian motion, the internal energy of a fluid particles is converted to heat energy that is responsible for maximum diffusion of temperature. Hence, with the higher values of Nb, the temperature characteristic upsurges is portrayed in Figure 4(d). The influence of α_e upon temperature profile is described in Figure 4(e). With the higher values of α_e, the augmenting behavior in temperature characteristic is perceived. Actually, with the growth in α_e, more time is required for heat to be diffused that gradually weakens the thermal layer at the boundary of flow system. Hence, with the growth in α_e, the temperature characteristic reduces, as depicted in Figure 4(e).

4.3 Concentration characteristics

The impacts of numerous factors on $\Phi(\eta)$ are described in Figure 5(a)–(f). The impact of concentration relaxation time factor α_c upon concentration profile is shown in Figure 5(a). A declining behavior is perceived in this figure. Similar to thermal relaxation time factor, more time is required for concentration to be diffused. Hence, with the upsurge in α_c, the concentration characteristic reduces as portrayed in Figure 5(a). The influence of activation energy factor E upon concentration profile is shown in Figure 5(b). It is observed in this figure that with the

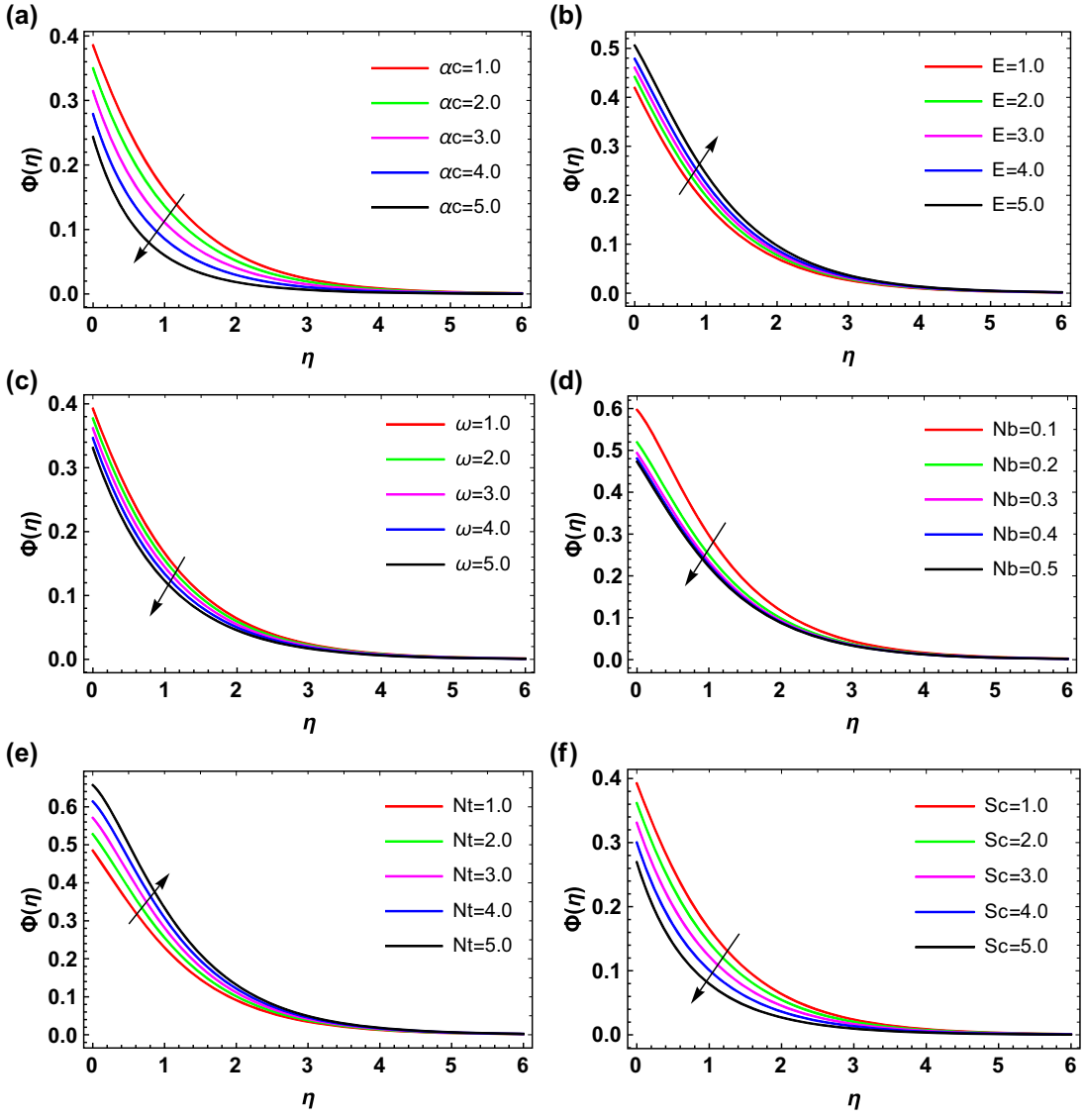

Figure 5: (a) Impact of α_c on concentration distribution $\Phi(\eta)$, (b) impact of activation energy factor E on concentration distribution $\Phi(\eta)$, (c) impact of chemical reaction factor ω on concentration distribution $\Phi(\eta)$, (d) impact of Brownian motion factor Nb on concentration distribution $\Phi(\eta)$, (e) impact of thermophoresis factor Nt on concentration distribution $\Phi(\eta)$, and (f) impact of Schmidt number Sc on concentration distribution $\Phi(\eta)$.

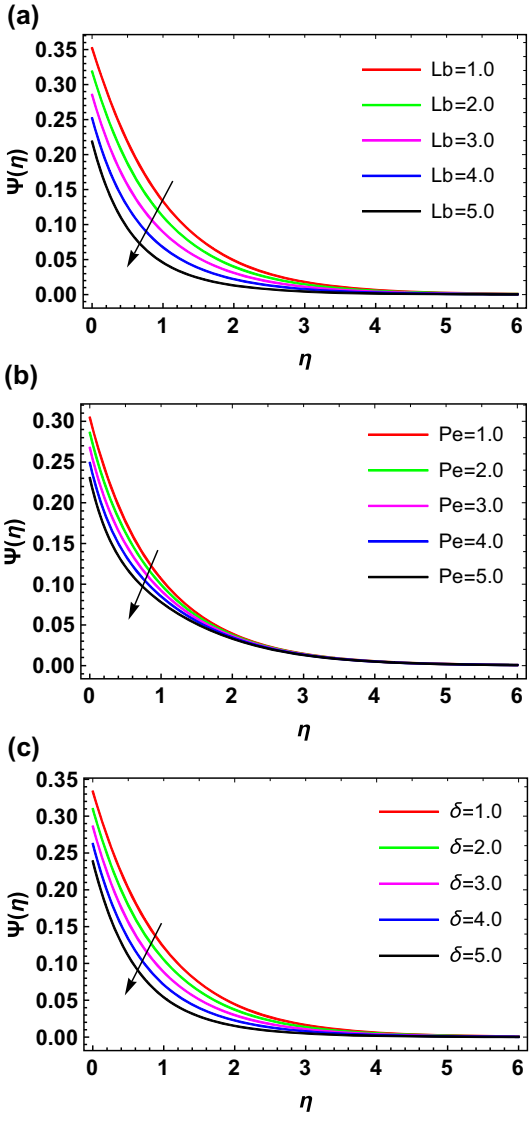

Figure 6: (a) Impact of bioconvection Lewis number Lb on microorganism concentration distribution $\psi(\eta)$, (b) impact of bioconvection Peclet number Pe on microorganism concentration distribution $\psi(\eta)$, and (c) impact of concentration difference factor δ on microorganism concentration distribution $\psi(\eta)$.

growth in E, there is an augmentation in concentration profile. Actually, the enhancement of E results in the decay of Arrhenius-modified function that eventually endorsed the generation of chemical reaction. In this physical process, the concentration of fluid particles upsurges as portrayed in Figure 5(b). The effect of chemical reaction factor ω upon concentration profile is portrayed in Figure 5(c). Actually, greater activation energy requirement is necessary for molecules to overcome the energy barriers and traverse the concentration gradients. In practical terms,

Table 1: Comparison of $\theta(0)$ with published results of Hassan *et al.* [60] for numerous values of Pr

Pr	Hassan *et al.* [60]	Present results
0.7	0.453945	0.453945
1.0	0.581992	0.581992
10.0	2.308013	2.308013

this manifests as a more pronounced resistance to the flow of substances, impacting various processes such as diffusion and chemical reactions. The augmented concentration profile reflects the increased energy investment needed for particles to overcome obstacles, indicating a more energetically demanding environment that influences the rate and efficiency of molecular transport and reactions within the system. Moreover, main reason for this change is that the number of solute molecules is experiencing chemically reactive effects and gets augmented with the growth in ω. In this process, the concentration characteristic diminishes. Figure 5(d) demonstrates the influence of Nb on concentration characteristic. In Figure 5(d), it is perceived that mass profile diminishes with the growing values of Nb. Actually with the upsurge in Nb, the zigzag motion among the fluid particles augments due to which more collisions among the nanoparticles occur. In this process, little mass disseminates and deteriorates the width of concentration boundary layer and ultimately reduced the concentration distribution. The impact of thermophoresis factor Nt upon concentration characteristic is shown in Figure 5(e). Here, it is perceived that growth

Table 2: Impacts of Rd, Nb, Nt, α_e, and Pr on $\frac{\mathrm{Nu}_x}{\sqrt{\mathrm{Re}_x}}$

Rd	Nb	Nt	α_e	Pr	$\frac{\mathrm{Nu}_x}{\sqrt{\mathrm{Re}_x}}$
0.2	0.5	0.5	0.5	1.0	0.1234453
0.6					0.1346787
0.7					0.1467897
0.8	0.6				0.5664464
	0.7				0.5568853
	0.8				0.5434674
	0.5	0.6			0.7654674
		0.7			0.7543567
		0.8			0.7432467
		0.5	0.6		0.3467753
			0.7		0.3346793
			0.8		0.3355324
			0.5	0.72	0.3976446
				2.0	0.4234675
				4.0	0.4568643

in Nt augments the concentration distribution. Actually, for upsurge in Nt, more mass diffuses, which strengthens the concentration boundary layer. Hence, with the upsurge in Nt, there is an augmentation in concentration distribution as depicted in Figure 5(e). The influence of Sc upon concentration distribution is portrayed in Figure 5(f). From this figure, it has observed that with the growing values of Sc, there is a retardation in concentration characteristic. Actually, higher values of Sc are related to the weaker solute diffusions, and the concentration characteristic declines for growth in Sc. Thus, the thickness of solute boundary is larger for smaller values of Sc, and *vice versa*. Finally, it should be noted that the movement of molecules inside fluids is known as convection. It is one of the primary techniques for transferring heat and mass, which uses diffusion and the random Brownian motion of various liquid components. Convection in this sense refers to all advective and diffusive transport combined. It is only interpreted as an advective phenomenon, though. Convective heat transfer is the process through which heat is transferred while fluids are moving in bulk. Heat that is being transmitted and dispersed is highlighted.

4.4 Microorganism characteristics

The effects of various factors on microorganism distribution $\psi(\eta)$ are shown in Figure 6(a)–(c). The impact of bioconvection Lewis number Lb upon $\psi(\eta)$ is depicted in Figure 6(a). Here, it is perceived that higher values of Lb diminish the microorganism panels. This can be explained, since Lb is in inverse relation to D_{n} (microorganisms diffusions) because of which for higher values of Lb there a retardation in microorganisms diffusion that deteriorates the strength of microbes layer at boundary. Therefore, with upsurge in Lb, there is a decline in $\psi(\eta)$ as depicted in Figure 6(a). The impression of Peclet number Pe on $\psi(\eta)$ is portrayed in Figure 6(b). Again, a reducing behavior in $\psi(\eta)$ is noted for higher values of Pe. This can be physically explained as *Wc* (speed of swimming cell) and Pe are inversely related to D_{n} (microorganism diffusions) and both are in direct relation. Moreover, the advection and diffusion rates are directly related to Pe. So, growth in Pe declines $\psi(\eta)$ as presented in Figure 6(b). The effect of concentration difference factor δ upon $\psi(\eta)$ is illustrated in Figure 6(c). In this figure, it is noted that with the growth in δ, $\psi(\eta)$ experiences a decline in their characteristic features due to intensified microbes' gradients. In fluid with substantial concentration differences, microorganisms face greater challenges in nutrient acquisition and energy utilization. The escalating gradient demands more efficient metabolic adaptations, potentially leading to a decline in growth rates and overall microbial vitality. This response reflects the organisms' struggle to maintain optimal physiological functions amid increasingly disparate concentrations, highlighting the complex relationship between fluid flow and microbial behavior in their quest for survival and proliferation. Actually, for upsurge in δ, the boundary-layer thickness of the microorganism distribution retards that ultimately reduces as depicted in Figure 6(c).

4.5 Table discussion

In Table 1, a comparative investigation has been conducted between our data and the results that are established by Hassan *et al.* [60]. A good agreement is noted between these results. In Table 2, the impacts of various factors upon Nusselt number are shown since the thermal diffusion is augmented with radiation and Brownian factors. Hence, these factors and Prandtl number are responsible to augment the Nusselt number, whereas higher values of thermophoresis and thermal relaxation time factors decline the Nusselt number. In Table 3, it is noted that with the growth in Schmidt number, thermophoresis, activation energy, and chemical reaction factors, the Sherwood number is reduced, while with the upsurge in Brownian and mass relaxation time factors, the Sherwood number is augmented. From Table 4, it is observed that for growth in bioconvective Lewis number, Peclet number, and concentration difference factor, the density number is declined.

Table 3: Impacts of Sc, Nb, Nt, α_{c}, E, and ω on $\frac{\mathrm{Sh}_x}{\sqrt{\mathrm{Re}_x}}$

Sc	Nb	Nt	α_{c}	E	ω	$\frac{\mathrm{Sh}_x}{\sqrt{\mathrm{Re}_x}}$
0.4	0.3	0.3	0.5	0.3	0.3	0.9432456
0.5						0.9345664
0.6						0.9245653
0.7	0.5					0.8975474
	0.6					0.9075464
	0.7					0.9124847
	0.3	0.5				0.8678535
		0.6				0.8578415
		0.7				0.8456780
		0.3	0.5			0.5535856
			0.6			0.5865364
			0.7			0.6134769
			0.5	0.5		0.8533456
				0.6		0.8456753
				0.7		0.8346851
				0.3	0.5	0.9643574
					0.6	0.9467898
					0.7	0.9236742

Table 4: Impacts of Lb, Pe, and δ on $\frac{\mathrm{Dn}_x}{\sqrt{\mathrm{Re}_x}}$

Lb	Pe	δ	$\frac{\mathrm{Dn}_x}{\sqrt{\mathrm{Re}_x}}$
0.1	0.1	0.1	0.8455364
0.2			0.8345767
0.3			0.8245795
0.1	0.2		0.9557742
	0.3		0.9432563
	0.4		0.9345775
	0.1	0.2	0.9532474
		0.3	0.9334565
		0.4	0.9124647

5 Conclusion

This work investigated the second-grade fluid flow over a stretching surface using convective constraints at boundary. The flow is affected by the magnetic effect in normal direction to the fluid motion. The fluid flow is influenced by thermal radiation and activation energy. The Cattaneo–Christov model of thermal and mass flux is also incorporated in this analysis. After detailed insight of the problem, it is observed that:

1) With rise in magnetic factor, the fluid motion has weakened. Also, an upsurge in second-grade fluid parameter results in a retardation in viscous forces, due to which fluid particles dislocate quite easily and quite frequently that causes growth in velocity of fluid.
2) For escalation in radiation factor, more heat diffuses, due to which maximum thermal transmission takes place from a zone of higher thermal concentration to a region of low thermal concentration. The higher values of Prandtl number have a declining impact upon thermal characteristics.
3) With the growth in thermophoresis factor, more heat diffuses that supports the strength of thermal boundary layer and boosts the temperature distribution.
4) With upsurge in Brownian motion, there are more collisions among the nanoparticles because more heat diffuses because during the growth in Brownian motion, the internal energy of fluid particles is converted into heat energy, which is responsible for maximum diffusion of temperature. With the growth in thermal relaxation time factor, more time is required for heat diffusion that gradually weakens the thermal boundary layer and declines the temperature profile.
5) With the upsurge in thermal relaxation time factor, more time is required for concentration to be diffused that declines the concentration profile. For greater effect activation energy and thermophoresis factors, there is an augmentation in concentration profiles. Upsurge in chemical reaction and Brownian motion factors are responsible for retardation in concentration characteristics. With the growth in Schmidt number, there is retardation in concentration characteristic.
6) The microorganisms' characteristics show a reducing behavior with growth in bioconvective Lewis, Peclet numbers, and concentration difference factor.
7) From the comparative analysis, a fine agreement exists between the existing and published results.

6 Future recommendations

In the future, this work can be extended for the three-dimensional second-grade fluid flows over a stretching surface. The authors can consider the slip conditions, convective condition, convective along with zero-mass flux conditions, *etc.* Additionally, some external forces such as magnetic field, porous medium, mixed convection, Joule heating, viscous dissipation, thermal-dependent heat source, and space-dependent heat source are also considered.

Funding information: This work was supported by the Deanship of Scientific Research, the Vice Presidency for Graduate Studies and Scientific Research, King Faisal University, Saudi Arabia (Grant No. 5843). The authors extend their appreciation to the Deanship of Scientific Research at King Khalid University, Abha, Saudi Arabia, for funding this work through the Research Group Project under Grant Number (RGP.2/505/44).

Author contributions: All authors have accepted responsibility for the entire content of this manuscript and approved its submission.

Conflict of interest: The authors state no conflict of interest.

Data availability statement: The data that support the findings of this study are available from the corresponding author upon a reasonable request.

References

[1] Biswal MM, Swain K, Dash GC, Ojha K. Study of radiative magneto-non-Newtonian fluid flow over a nonlinearly elongating sheet with Soret and Dufour effects. Numer Heat Transf Part A Appl. 2023;83:331–42.

[2] Iqbal Z, Khan M, Shoaib M, Ahammad NA, Sidi MO. Heat transport analysis in buoyancy-driven flow of Maxwell fluid induced by a vertically stretching sheet inspired by Cattaneo Christov theory. Waves Random Complex Media. 2022;1–13.
[3] Sharma RP, Shaw S. MHD Non-Newtonian fluid flow past a stretching sheet under the influence of non-linear radiation and viscous dissipation. J Appl Comput Mech. 2022;8:949–61.
[4] Iqbal Z, Saleem M. Convective heat transport features of Darcy Casson fluid flow in a vertical channel: a Lie group approach. Waves Random Complex Media. 2022;1–14.
[5] Khalil KM, Soleiman A, Megahed AM, Abbas W. Impact of variable fluid properties and double diffusive Cattaneo–Christov model on dissipative Non-Newtonian fluid flow due to a stretching sheet. Mathematics. 2022;10:1179.
[6] Nandi S, Iqbal Z, Alhagyan M, Ahammad NA, Albasheir NAM, Gargouri A, et al. Computational assessment of MHD Carreau tri-hybrid nano-liquid flow along an elongating surface with entropy generation: A comparative study. Case Stud Therm Eng. 2023;50:103420.
[7] Asogwa KK, Goud BS, Reddy YD. Non-Newtonian electromagnetic fluid flow through a slanted parabolic started Riga surface with ramped energy. Heat Transf. 2022;51:5589–606.
[8] Farahani SD, Hosseni M, Zakinia A, Öztop HF. Control of non-Newtonian fluid flow and heat transfer in microchannel by using porous triangular ribs and pulsating jet. Eur Phys J Plus. 2022;137:737.
[9] Rehman S, Muhammad N. Mathematical analysis of nonlinear models and their role in dynamics. Mod Phys Lett B. 2023;2450097.
[10] Fourier JBJ. Théorie analytique de la chaleur. Chez Firmin Didot, père et fils; 1822.
[11] Fick A. On liquid diffusion. J Memb Sci. 1995;100:33–8.
[12] Cattaneo C. Sulla conduzione del calore. Atti Sem Mat Fis Univ Modena. 1948;3:83–101.
[13] Christov CI. On frame indifferent formulation of the Maxwell–Cattaneo model of finite-speed heat conduction. Mech Res Commun. 2009;36:481–6.
[14] Waqas H, Fida M, Liu D, Manzoor U, Muhammad T. Numerical simulation of entropy generation for nanofluid with the consequences of thermal radiation and Cattaneo-Christov heat flux model. Int Commun Heat Mass Transf. 2022;137:106293.
[15] Gireesha BJ, Shankaralingappa BM, Prasannakumar BC, Nagaraja B. MHD flow and melting heat transfer of dusty Casson fluid over a stretching sheet with Cattaneo–Christov heat flux model. Int J Ambient Energy. 2022;43:2931–9.
[16] Reddy PS, Sreedevi P, Chamkha AJ. Heat and mass transfer analysis of nanofluid flow over swirling cylinder with Cattaneo–Christov heat flux. J Therm Anal Calorim. 2022;147:3453–68.
[17] Asghar Z, Kousar M, Waqas M, Irfan M, Bilal M, Khan WA. Heat generation in mixed convected Williamson liquid stretching flow under generalized Fourier concept. Appl Nanosci. 2020;10:4439–44.
[18] Khan MWS, Ali N, Asghar Z. Thermal and rheological effects in a classical Graetz problem using a nonlinear Robertson-Stiff fluid model. Heat Transf. 2021;50:2321–38.
[19] Yaseen M, Rawat SK, Kumar M. Cattaneo–Christov heat flux model in Darcy–Forchheimer radiative flow of MoS2–SiO2/kerosene oil between two parallel rotating disks. J Therm Anal Calorim. 2022;147:10865–87.
[20] Eswaramoorthi S, Loganathan K, Jain R, Gyeltshen S. Darcy-Forchheimer 3D flow of glycerin-based carbon nanotubes on a Riga plate with nonlinear thermal radiation and Cattaneo-Christov heat flux. J Nanomater. 2022;2022:1–20.
[21] Alharbi KAM, Alshahrani MN, Ullah N, Khan NM, Marek K, Mousa AAA, et al. Cattaneo–Christov heat flow model for copper–water nanofluid heat transfer under Marangoni convection and slip conditions. Sci Rep. 2022;12:1–12.
[22] Magodora M, Mondal H, Sibanda P. Effect of Cattaneo-Christov heat flux on radiative hydromagnetic nanofluid flow between parallel plates using spectral quasilinearization method. J Appl Comput Mech. 2022;8:865–75.
[23] Rana P, Mackolil J, Mahanthesh B, Muhammad T. Cattaneo-Christov Theory to model heat flux effect on nanoliquid slip flow over a spinning disk with nanoparticle aggregation and Hall current. Waves Random Complex Media. 2022;1–23.
[24] Reza-E-Rabbi S, Ahmmed SF, Islam S, Arifuzzaman SM, Rana BMJ, Ali MY, et al. Characterization of fluid flow and heat transfer of a periodic magnetohydrodynamics nano non-Newtonian liquid with Arrhenius activation energy and nonlinear radiation. Heat Transf. 2022;51:6578–615.
[25] Zeeshan A, Mehmood OU, Mabood F, Alzahrani F. Numerical analysis of hydromagnetic transport of Casson nanofluid over permeable linearly stretched cylinder with Arrhenius activation energy. Int Commun Heat Mass Transf. 2022;130:105736.
[26] Khan A, Saeed A, Tassaddiq A, Gul T, Mukhtar S, Kumam P, et al. Bio-convective micropolar nanofluid flow over thin moving needle subject to Arrhenius activation energy, viscous dissipation and binary chemical reaction. Case Stud Therm Eng. 2021;25:100989.
[27] Azam M. Effects of Cattaneo-Christov heat flux and nonlinear thermal radiation on MHD Maxwell nanofluid with Arrhenius activation energy. Case Stud Therm Eng. 2022;34:102048.
[28] Kumar A, Ray RK, Sheremet MA. Entropy generation on double-diffusive MHD slip flow of nanofluid over a rotating disk with nonlinear mixed convection and Arrhenius activation energy. Indian J Phys. 2022;96:525–41.
[29] Bhatti MM, Arain MB, Zeeshan A, Ellahi R, Doranehgard MH. Swimming of gyrotactic microorganism in MHD Williamson nanofluid flow between rotating circular plates embedded in porous medium: Application of thermal energy storage. J Energy Storage. 2022;45:103511.
[30] Upreti H, Pandey AK, Uddin Z, Kumar M. Thermophoresis and Brownian motion effects on 3D flow of Casson nanofluid consisting microorganisms over a Riga plate using PSO: A numerical study. Chin J Phys. 2022;78:234–70.
[31] Ma J. Thermal examination for the micropolar gold ± blood nanofluid flow through a permeable channel subject to gyrotactic microorganisms. Future. 2022;1:1–2.
[32] Khan A, Saeed A, Tassaddiq A, Gul T, Kumam P, Ali I, et al. Bio-convective and chemically reactive hybrid nanofluid flow upon a thin stirring needle with viscous dissipation. Sci Rep. 2021;11:1–17.
[33] Faizan M, Ali F, Loganathan K, Zaib A, Reddy CA, Abdelsalam SI. Entropy analysis of Sutterby nanofluid flow over a riga sheet with gyrotactic microorganisms and Cattaneo–Christov double diffusion. Mathematics. 2022;10:3157.
[34] Madhukesh JK, Ramesh GK, Aly EH, Chamkha AJ. Dynamics of water conveying SWCNT nanoparticles and swimming microorganisms over a Riga plate subject to heat source/sink. Alex Eng J. 2022;61:2418–29.
[35] Rehman KU, Shatanawi W, Al-Mdallal QM. A comparative remark on heat transfer in thermally stratified MHD Jeffrey fluid flow with

thermal radiations subject to cylindrical/plane surfaces. Case Stud Therm Eng. 2022;32:101913.
[36] Hussain SM, Goud BS, Madheshwaran P, Jamshed W, Pasha AA, Safdar R, et al. Effectiveness of nonuniform heat generation (sink) and thermal characterization of a Carreau fluid flowing across a nonlinear elongating cylinder: A numerical study. ACS Omega. 2022;7:25309–20.
[37] Shaw S, Samantaray S, Misra A, Nayak MK, Makinde OD. Hydromagnetic flow and thermal interpretations of Cross hybrid nanofluid influenced by linear, nonlinear and quadratic thermal radiations for any Prandtl number. Int Commun Heat Mass Transf. 2022;130:105816.
[38] Lone SA, Alyami MA, Saeed A, Dawar A, Kumam P, Kumam W. MHD micropolar hybrid nanofluid flow over a flat surface subject to mixed convection and thermal radiation. Sci Rep. 2022;12:1–14.
[39] Ibrahim M, Saeed T, Zeb S. Numerical simulation of time-dependent two-dimensional viscous fluid flow with thermal radiation. Eur Phys J Plus. 2022;137:609.
[40] Bilal M, Saeed A, Gul T, Kumam W, Mukhtar S, Kumam P. Parametric simulation of micropolar fluid with thermal radiation across a porous stretching surface. Sci Rep. 2022;12:1–11.
[41] Dogonchi AS, Asghar Z, Waqas M. CVFEM simulation for Fe3O4-H2O nanofluid in an annulus between two triangular enclosures subjected to magnetic field and thermal radiation. Int Commun Heat Mass Transf. 2020;112:104449.
[42] Khan WA, Waqas M, Chammam W, Asghar Z, Nisar UA, Abbas SZ. Evaluating the characteristics of magnetic dipole for shear-thinning Williamson nanofluid with thermal radiation. Comput Methods Prog Biomed. 2020;191:105396.
[43] Waqas M, Khan WA, Asghar Z. An improved double diffusion analysis of non-Newtonian chemically reactive fluid in frames of variables properties. Int Commun Heat Mass Transf. 2020;115:104524.
[44] Haq F, Kadry S, Chu Y-M, Khan M, Khan MI. Modeling and theoretical analysis of gyrotactic microorganisms in radiated nanomaterial Williamson fluid with activation energy. J Mater Res Technol. 2020;9:10468–77.
[45] Waqas M, Akram N, Asghar Z, Gulzar MM, Javed MA. An improved Darcian analysis for chemically reacted Maxwell liquid toward convectively heated moving surface with magnetohydrodynamics. J Therm Anal Calorim. 2021;143:2069–74.
[46] Adnan, Iqbal Z, Elattar S, Abbas W, Alhazmi SE, Yassen MF. Thermal enhancement in buoyancy-driven stagnation point flow of ternary hybrid nanofluid over vertically oriented permeable cylinder integrated by nonlinear thermal radiations. Int J Mod Phys B. 2023;37:2350215.
[47] Turkyilmazoglu M. Three dimensional viscous flow due to a squeezing porous slider. Eur J Mech. 2023;98:253–9.
[48] Rahman M, Sharif F, Turkyilmazoglu M, Siddiqui MS. Unsteady three-dimensional magnetohydrodynamics flow of nanofluids over a decelerated rotating disk with uniform suction. Pramana. 2022;96:170.
[49] Turkyilmazoglu M. Heat transfer enhancement feature of the Non-Fourier Cattaneo–Christov heat flux model. J Heat Transf. 2021;143:94501.
[50] Muhammad N, Alharbi KAM. OpenFOAM for computational hydrodynamics using finite volume method. Int J Mod Phys B. 2023;37:2350026.
[51] Liao S-J. An explicit, totally analytic approximate solution for Blasius' viscous flow problems. Int J Nonlinear Mech. 1999;34:759–78.
[52] Liao S. An optimal homotopy-analysis approach for strongly nonlinear differential equations. Commun Nonlinear Sci Numer Simul. 2010;15:2003–16.
[53] Shamshuddin MD, Akkurt N, Saeed A, Kumam P. Radiation mechanism on dissipative ternary hybrid nanoliquid flow through rotating disk encountered by Hall currents: HAM solution. Alex Eng J. 2023;65:543–59.
[54] Kumar A, Yadav PK. Entropy generation analysis of non-miscible couple stress and Newtonian fluid in an inclined porous channel with variable flow properties: HAM Analysis. Int J Mod Phys B. 2023;2450390.
[55] Mabood F, Shamshuddin MD, Mishra SR. Characteristics of thermophoresis and Brownian motion on radiative reactive micropolar fluid flow towards continuously moving flat plate: HAM solution. Math Comput Simul. 2022;191:187–202.
[56] Mandal DK, Biswas N, Manna NK, Gorla RSR, Chamkha AJ. Role of surface undulation during mixed bioconvective nanofluid flow in porous media in presence of oxytactic bacteria and magnetic fields. Int J Mech Sci. 2021;211:106778.
[57] Shehzad SA, Hayat T, Alsaedi A, Meraj MA. Cattaneo-Christov heat and mass flux model for 3D hydrodynamic flow of chemically reactive Maxwell liquid. Appl Math Mech. 2017;38:1347–56.
[58] Veena PH, Suresh B, Pravin VK, Goud AM. Non-Newtonian momentum transfer past an isothermal stretching sheet with applied suction. Int J Appl Mech Eng. 2017;22:665–74.
[59] Dawar A, Islam S, Shah Z, Mahmuod SR. A passive control of Casson hybrid nanofluid flow over a curved surface with alumina and copper nanomaterials: A Study on Sodium Alginate-Based Fluid. J Mol Liq. 2023;382:122018.
[60] Hassan HS, Mahrous SA, Sharara A, et al. A study for MHD boundary layer flow of variable viscosity over a heated stretching sheet via Lie-group method. Appl Math Inf Sci. 2015;9:1327.